

# Avoiding Deadlocks Is Not Enough: Analysis and Resolution of Blocked Airplanes

Shuhao Qi<sup>1</sup>, Zengjie Zhang<sup>1</sup>, Zhiyong Sun<sup>2</sup> and Sofie Haesaert<sup>1</sup>

**Abstract**—The foreseen increased usage of unmanned airplanes has been shown to lead to the emergence of pathological phenomena referred to as *blocking* in which airplanes stick together and fly in parallel for a long time. Although *deadlock*, a well-known pathological phenomenon in multi-agent systems, has been widely studied, it does not cover this temporal blocking phenomenon. As airspace becomes not only more autonomous but also increasingly crowded, and accommodates various types of aircraft, the blocking phenomenon is likely to occur even more frequently and negatively impact airplane systems. Therefore, it is crucial to understand and address the blocking phenomenon carefully in control design. To analyze blocking, we model airplane avoidance controllers using safety filters and examine the underlying causes in a two-airplane encounter situation. Furthermore, we propose an intention-aware strategy that efficiently resolves this pathological behavior while incidentally addressing deadlocks. Notably, the developed strategy does not rely on central coordination and communications which become unreliable in harsh situations. The analytical results are based on a simple dynamic model for airplanes, while the proposed resolution strategy is verified in both this simple model and a more realistic one.

## I. INTRODUCTION

With the rising demand for aviation services, public airspace not only becomes increasingly crowded but also must accommodate a mix of manned and unmanned vehicles [1]. Therefore, encounter situations between aircraft are becoming more frequent in the future airspace [2]. This trend challenges conventional air traffic management (ATM) systems that rely on central ground coordinators which scale poorly for large-scale traffic [3]. In this context, the next generation of autonomous ATM aims to enable airplanes to coordinate themselves in a decentralized manner [4]. Without central coordination, collision avoidance heavily relies on the detect and avoid (DAA) systems [5], [6], which allows aircraft to detect potential collisions and take evasive actions to avoid the other aircraft. Nevertheless, DAA systems may suffer from possible conflicts between safety and task accomplishment [6]. In this paper, safety refers to free collision, while task accomplishment refers to target reaching. In such safety-critical systems, safety is typically prioritized over task accomplishment, leading to the possible sacrifice of task performance. This trade-off results in so-called pathological phenomena [7], where agents fail to achieve their tasks as expected.

This work was supported by the European project SymAware under the grant No. 101070802, and by the European project COVER under the grant No. 101086228.

<sup>1</sup> S. Qi, Z. Zhang, S. Haesaert are with the Department of Electrical Engineering, Eindhoven University of Technology, Eindhoven, The Netherlands. {s.qi, z.zhang3, s.haesaert}@tue.nl

<sup>2</sup> Z. Sun is with the College of Engineering, Peking University, Beijing, China. {zhiyong.sun@pku.edu.cn}

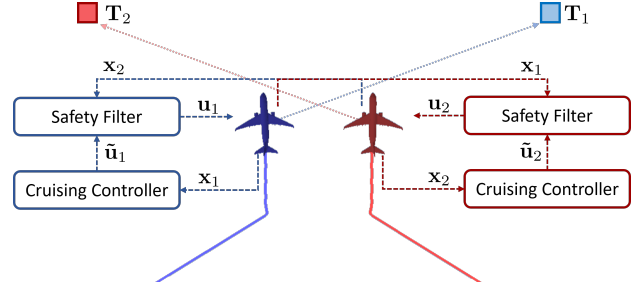


Fig. 1: Blocking phenomenon in a two-airplane system. The colored lines represent the trajectories of airplanes toward the target positions represented by square markers.

A typical pathological behavior is deadlock [8]–[10], where all agents get stuck in a static configuration before reaching targets. Theoretical results have shown that multi-agent systems with decentralized safety-critical controllers, like control barrier function (CBF) [9], [11], model predictive control (MPC) [12], and safe-reachable set [13] tend to cause deadlocks. Deadlock can be regarded as an undesired equilibrium [8], [14], arising from the compromise of target reachability to safety constraints. Meanwhile, another similar but different pathological phenomenon is *livelock* [7], where agents keep moving but never reach their targets. Although deadlocks and livelocks have attracted much attention in existing literature, it has been shown that true deadlocks and livelocks are very rare in practice and only occur in very strict conditions [9], for example, symmetric configurations [15].

Instead, a much more common and dangerous phenomenon is what we refer to as a *blocking*, where agents are blocked for a finite time. In a high-fidelity air-traffic simulation of encounter scenarios, the Netherlands Aerospace Centre has reported a phenomenon where two airplanes repeatedly strive but fail to bypass each other, resulting in parallel flight for a finite time [6]. In this paper, we use CBF-based safety filters to represent the DAA systems of airplanes, and also observe a finite-time parallel-flying phenomenon illustrated in Fig. 1. The concepts of deadlock, livelock, and blocking were initially studied in software systems [16] that are defined over discrete-state space. In discrete-state systems, *blocking* is used to distinguish from endless deadlock and livelock [16]–[18]. Inspired by this, we refer to the finite-time parallel flying of blocked airplanes depicted in Fig. 1 within continuous-state space as the *blocking mode* in this paper. Such the blocking phenomenon not only hinders the target-reaching progress but also contributes to the increased near misses between airplanes, particularly under realistic uncertainty. The foreseen increased usage of unmanned airplanes led to the emergence of the blocking phenomena. Therefore, it is crucial to study

this blocking phenomenon thoroughly. This paper will present an exploratory study on characterizing and analyzing the blocking phenomenon, and then propose a resolution strategy to mitigate it.

While blocking resolution in continuous dynamic systems is not discussed, existing approaches for well-studied deadlock resolution offer promising extensions to address the blocking phenomenon. Deadlock resolution methods can be categorized into four main approaches: 1) Central coordination, where a central coordinator manages agent interactions to resolve deadlocks [19], [20]. However, this method is incompatible with the decentralized configuration considered in this paper. 2) Reactive distributed controllers, which rely on local communication to negotiate with nearby airplanes, using techniques such as parametric control Lyapunov functions [21] and rotation controllers for position swaps [9], [22]. These methods assume stable and instantaneous communication, which can be difficult to establish in practice [23], particularly between different types of aircraft. Given the safety-critical requirements, airplanes should ensure both safety and task accomplishment independently, even without communication. 3) Perturbation addition, which involves introducing disruptions to break deadlock conditions [11]. While perturbation is a practical solution to break strict deadlock conditions, it does not guarantee deadlock resolution and can compromise safety constraints. 4) Predefined rules and priorities, such as right-hand priority rules [24], [25], predefined curved maneuvers [26], or stopping strategies [27], can be encoded directly into controllers. However, these fixed approaches can lead to inefficiencies or unnecessary losses. To meet the demands of future airspace, we attempt to propose an efficient and guaranteed resolution strategy without relying on central coordination and communication. An important observation is that human walkers or drivers can resolve conflicts easily without communication, even in crowded situations, by exhibiting their intentions and estimating the intentions of surrounding agents. Inspired by this, we propose an intention-aware strategy that generates an adaptive priority of unblocking behavior, which provides guarantees and also improves efficiency.

The key contributions of this paper are: 1) Analyzing why DAA systems lead to blocking modes using safety filters for simplified airplane models; 2) Developing an efficient and certified resolution framework that operates without communication. To the best of our knowledge, this is the first work to discuss the finite-time blocking phenomenon in continuous-state systems. An important insight from this study reveals that pathological behavior typically occurs when two airplanes simultaneously choose symmetric avoidance maneuvers under the principle of optimality, preventing them from agreeing on how to resolve the conflict. Although behavior varies across different system dynamics, similar phenomena share common characteristics across various systems. Therefore, we believe this work provides valuable insights not only for practical air traffic systems but also for a wide range of applications, including autonomous driving and robot navigation in the crowd.

In this paper, vector variables will be given as bold symbols,  $\mathbf{x} \in \mathbb{R}^n$ , while scalars will be denoted as  $x \in \mathbb{R}$ .  $\|\cdot\|$

denotes Euclidean norm of a vector. Furthermore, we defined the following angular normalization operator which maps an angle  $a \in \mathbb{R}$  to the range  $[-\pi, \pi)$

$$\angle(a) = (a + \pi) \% 2\pi - \pi, \quad (1)$$

where  $\%$  is the modulo operator.

## II. PROBLEM STATEMENT AND SYSTEM MODELING

This paper considers a horizontal two-airplane system in an encounter scenario. Each airplane is equipped with a cruising controller that generates inputs heading towards the target and a DAA system that adjusts the cruising control law to avoid the other airplane. We aim to develop a strategy capable of resolving not only deadlock and livelock but also the phenomenon illustrated in Fig. 1. To meet the demands of future air traffic, the resolution strategy must be efficient, guaranteed, and effective without relying on central coordination and communications. Subsequently, we will introduce the formulation of the system and controllers, the configuration of the encounter scenario, and then present a formal definition of the blocking phenomenon.

### A. Two-airplane dynamic systems

We consider a system consisting of two dynamic airplanes,  $\mathcal{A} = \{A_1, A_2\}$ , operating in a horizontal plane. Each airplane is modeled as a single integrator model with constant speed,

$$A_i : \quad \dot{\mathbf{x}}_i = \underbrace{\begin{bmatrix} v \cos(\theta_i) \\ v \sin(\theta_i) \end{bmatrix}}_{\mathbf{u}_i}, \quad i \in \{1, 2\}, \quad (2)$$

where  $\mathbf{x}_i, \mathbf{u}_i \in \mathbb{R}^2$  respectively denote the horizontal position and velocity for  $A_i$ . Given  $v \in \mathbb{R}_{>0}$  is a constant speed, the actual control input is the heading angle,  $\theta_i$ . We say that  $\mathbf{x}_i(t) : \mathbb{R}_{\geq 0} \rightarrow \mathbb{R}^2$  is a solution of (2) initialized at  $\mathbf{x}_i(0)$ . The model (2) is simplified from a unicycle model with constant speed [28] commonly used to represent the horizontal behavior of fixed-wing aircraft. Besides the dynamics in (2), a unicycle model would also include the angular velocity  $\dot{\theta}_i$  to capture the dynamics of the heading angle. While the model in (2) can replicate the smooth unicycle-like trajectories, it allows for instantaneous turns that are infeasible in a unicycle model and real airplanes. However, for simplicity, this paper analyzes the blocking phenomenon using the single integrator in Eq. (2) since the analysis based on the heading angle  $\theta_i$  is more intuitive than one based on angular velocity  $\dot{\theta}_i$ . The obtained results for the model (2) are also applicable to the unicycle model, which will be demonstrated in Sec. V.

Fig. 2 depicts a two-airplane system in a sketch. The joint state of the two-airplane system is given as  $\mathbf{x} := \begin{bmatrix} \mathbf{x}_1 \\ \mathbf{x}_2 \end{bmatrix}$ . In this paper, we assume that  $A_1$  and  $A_2$  have a consistent speed,  $v$ . Each airplane can accurately observe the other's current state and previous heading angle; however, the other airplane's current input and heading angle is unknown. Each airplane aims at reaching its target destination, denoted as  $\mathbf{T}_i$  for  $A_i$ ,  $i \in \{1, 2\}$ . Two angles are introduced: 1) The relative angle,  $\beta_i$ , denotes the angle of the other airplane,  $A_j$ , relative to  $A_i$ , i.e.,  $\begin{bmatrix} \cos(\beta_i) \\ \sin(\beta_i) \end{bmatrix} = \frac{\mathbf{x}_j - \mathbf{x}_i}{\|\mathbf{x}_j - \mathbf{x}_i\|}$ , for  $i, j \in \{1, 2\}, i \neq j$ . 2) The cruising angle denoted by  $\phi_i$  points to its corresponding target

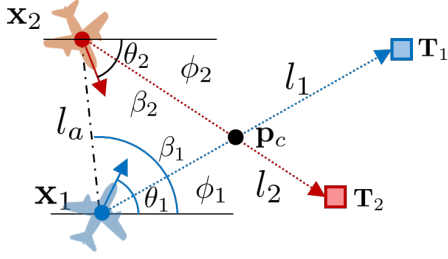


Fig. 2: The sketch of a two-airplane system. The solid dots represent the current positions of airplanes,  $\mathbf{x}_1$  and  $\mathbf{x}_2$ , while rectangle markers indicate their target locations,  $\mathbf{T}_1$  and  $\mathbf{T}_2$ . For each airplane three key angles are shown: the heading angle  $\theta_i$ , the relative angle  $\beta_i$ , and the cruising angle  $\phi_i$ . Three line segments are illustrated:  $l_a$  connecting two airplanes,  $l_1$  connecting  $\mathbf{x}_1$  and  $\mathbf{T}_1$ , and  $l_2$  connecting  $\mathbf{x}_2$  and  $\mathbf{T}_2$ . The intersection point between  $l_1$  and  $l_2$  is denoted by  $\mathbf{p}_c$ .

point  $\mathbf{T}_i$  from the current position, i.e.,  $\begin{bmatrix} \cos(\phi_i) \\ \sin(\phi_i) \end{bmatrix} = \frac{\mathbf{T}_i - \mathbf{x}_i}{\|\mathbf{T}_i - \mathbf{x}_i\|}$ . In the following discussion, changes of the heading angle in different situations are seamlessly linked to these two angles.

To ensure safety, the relative distance between two airplanes should satisfy

$$h(\mathbf{x}) = \|\mathbf{x}_1 - \mathbf{x}_2\|^2 - r^2, \quad (3)$$

where  $r$  denotes the safe distance between airplanes. Furthermore, the collision-free set is defined as  $\mathcal{C} := \{\mathbf{x} \mid h(\mathbf{x}) > 0\}$ . As shown in Fig. 1, we consider that each airplane has a control system with two components: a cruising controller to navigate to its target and a safety filter to avoid collision. The cruising controller of  $A_i$  is naturally designed as,

$$\mathcal{N} : \tilde{\mathbf{u}}_i = \begin{cases} v \frac{\mathbf{T}_i - \mathbf{x}_i}{\|\mathbf{T}_i - \mathbf{x}_i\|}, & \mathbf{x}_i \neq \mathbf{T}_i \\ \mathbf{0}, & \mathbf{x}_i = \mathbf{T}_i \end{cases}, \quad (4)$$

for  $i \in \{1, 2\}$ . With this controller, airplanes will head to targets straightly before reaching targets and then stop at the target. We say  $A_i$  is in *cruising mode* when  $\mathbf{u}_i = \tilde{\mathbf{u}}_i$ , i.e.,  $\theta_i = \phi_i$ . However, the cruising control law may violate the safety constraints in Eq. (3) in encounter situations as defined as follows,

**Definition 1** (Encounter situation). *Given a two-airplane system in which  $A_i$  flies from  $\mathbf{x}_i(0)$  to  $\mathbf{T}_i$  for  $i \in \{1, 2\}$ , the two airplane will encounter each other if  $\exists t \in [t_0, \infty)$ ,  $h(\mathbf{x}(t)) < 0$  when both airplanes take the cruising control law in Eq. (4), i.e.,  $\mathbf{u}_1 = \tilde{\mathbf{u}}_1$  and  $\mathbf{u}_2 = \tilde{\mathbf{u}}_2$ . We assume initial and target positions of two airplanes satisfy the safety constraints, i.e.,  $\|\mathbf{x}_1(0) - \mathbf{x}_2(0)\|^2 - r^2 \geq 0$  and  $\|\mathbf{T}_1 - \mathbf{T}_2\|^2 - r^2 \geq 0$ .*

In Fig. 2,  $\mathbf{p}_c$  is regarded as the encounter point of two airplanes. To handle encounter situations, a collision-avoidance controller, such as DAA system in airplanes, is necessary to ensure collision-free safety. Given the complexity of real-world DAA systems [5], which makes them difficult to analyze, we must develop a more analyzable model to capture the avoidance behavior generated by DAA systems. Therefore, we propose a safety filter [29] of  $A_i$  that detects unsafe cruising control inputs and modifies them with minimal interference to ensure  $\mathbf{x} \in \mathcal{C}$ , which is formulated as a quadratic programming

problem,

$$\mathcal{F} : \underset{\mathbf{u}_i \in \mathbb{R}^2}{\operatorname{argmin}} \quad \frac{1}{2} \|\mathbf{u}_i - \tilde{\mathbf{u}}_i\|^2 \quad (5a)$$

$$\text{s.t.} \quad \frac{\alpha}{2} h(\mathbf{x}) + 2(\mathbf{x}_i - \mathbf{x}_j)^T \mathbf{u}_i \geq 0 \quad (5b)$$

$$\|\mathbf{u}_i\| = v, \quad (5c)$$

for  $i \neq j$  and  $i, j \in \{1, 2\}$ . Eq. (5b) is a decentralized CBF condition based on the half-responsibility assumption, which is used in [9], [11], [30]. The derivation of Eq. (5b) can be found in Appendix A. Due to the minimal interference manner of the objective function in Eq. (5a), the safety filter corrects the cruising control inputs only when they are discerned as unsafe and, otherwise, maintains the cruising control law, which is similar to DAA systems. In this paper, the safety filter is regarded as being *activated* when  $\mathbf{u} \neq \tilde{\mathbf{u}}$ . Assuming the safety filters of two airplanes have uniform parameters of  $\alpha$  and  $r$ , the model formulated above exhibits a phenomenon of parallel flying similar to Fig. 3 and 4 in [6].

### B. Blocking mode

In an encounter situation, the safety filters will be activated as airplanes approach the encounter point. Although the safety filter in Eq. (5) helps to resolve some conflicts, the collision-avoiding behavior generated by the safety filter does not guarantee a definite resolution of conflicts. In certain situations, the controller may sacrifice the target convergence to ensure safety, resulting in non-convergence pathological phenomena like typical deadlock and livelock phenomena.

**Definition 2** (Deadlock [9] and Livelock [7]). *An agent is in a deadlock at time  $t_0$  when  $\exists \mathbf{P} \in \mathbb{R}^2$ ,  $\mathbf{x}(t) = \mathbf{P} \neq \mathbf{T}$  for all  $t > t_0$ . An agent is in a livelock at time  $t_0$  if  $\forall t > t_0$ ,  $\mathbf{x}(t) \neq \mathbf{T}$  and  $\dot{\mathbf{x}}(t) \neq \mathbf{0}$ .*

As discussed in the introduction, the finite-time blocking phenomenon illustrated in Fig. 1 is both common and hazardous for airplane systems. If not resolved infinitely, blocking may deteriorate into deadlock or livelock in some systems. To address this issue, we formally define the *blocking mode* tailored to the two-airplane systems.

**Definition 3** (Blocking mode).  *$A_i \in \mathcal{A}$  is in blocking mode at  $t_0$  if  $\mathbf{u}_i(t_0) \neq \tilde{\mathbf{u}}_i(t_0)$  and  $\omega(t_0) = 0$ , where  $\omega := \frac{(\mathbf{x}_1 - \mathbf{x}_2) \times (\mathbf{u}_1 - \mathbf{u}_2)}{\|\mathbf{x}_1 - \mathbf{x}_2\|^2}$  is the angular velocity of  $A_1$  relative to  $A_2$ .*

$\omega = 0$  indicates that the two airplanes are flying parallel to each other, as depicted in Fig. 1.

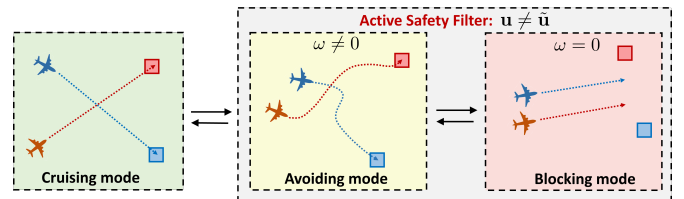


Fig. 3: Three modes of an airplane in an encounter.

In an encounter situation, rotating around each other to swap positions can effectively resolve it, which is widely used in conflict resolution [9], [21], [22], [26]. In other

words, encounter conflicts can be resolved within a finite time by continuous unidirectional rotation of the two airplanes. Consequently,  $\omega$  can be used as an indicator to determine whether the system performs effective resolution.  $\omega = 0$  prolongs conflict resolution, whereas a larger  $\omega$  leads to more efficient conflict resolution. Contrary to the blocking mode with  $\omega = 0$ ,  $A_i$  is regarded as being in *avoiding mode* if  $\mathbf{u}_i(t) \neq \tilde{\mathbf{u}}_i(t)$  and  $\omega(t) \neq 0$ , indicating this airplane performs effective behavior to resolve the conflicts. As shown in Fig. 3, an airplane will switch among three modes in an encounter.

### III. ANALYSIS OF BLOCKING MODE

This section begins by presenting an explicit solution of the safety filter in Eq. (5), illustrating how safety filters function during the flight. Using the explicit solution, we derive the conditions under which blocking modes occur. This allows us to estimate the blocking duration to quantify its potential impact in advance. In addition, we briefly introduce possible occurrences of deadlock and livelock. These results facilitate the design of resolution methods in the next section.

#### A. Explicit solutions of safety filter

When two airplanes are sufficiently far apart, airplanes can choose any admissible control inputs, which means all the control inputs in  $\{\mathbf{u} \mid \|\mathbf{u}\| = v\}$  satisfy the CBF condition in (5b). We refer to this situation as the *free flight* phase. The condition of the free flight phase is related to the distance between two airplanes denoted as  $d_{1,2} = \|\mathbf{x}_2 - \mathbf{x}_1\|$ , which is derived from (5b),

$$d_{1,2} > \frac{2v}{\alpha} + \sqrt{\frac{4v^2}{\alpha^2} + r^2},$$

When the airplanes come closer, not all control inputs remain safe. Because airplanes maintain a constant speed, their control inputs are determined by their heading angles; Thus, we primarily analyze safe and unsafe inputs based on these heading angles. Fig. 4 illustrates how the safety filter functions. The green arc denotes the set of safe heading angles, while the red and yellow arcs represent the unsafe heading angle set. The red and yellow arc is symmetric to the line between two airplanes,  $l_a$ , with an identical angular range denoted as  $\Delta$ . Hence, the unsafe set is characterized by  $\|\angle(\phi_i - \beta_i)\| < \Delta$ . In the free flight phase,  $\Delta_i = 0$ . As the airplanes approach each other,  $\Delta$  increase with decreasing  $d_{1,2}$  and gradually converge to  $\frac{\pi}{2}$ . Due to the minimal interference manner, the safety filter will correct  $\tilde{\mathbf{u}}_i$  to the nearest boundary in the safe set, i.e.,  $\beta_i + \Delta_i$  or  $\beta_i - \Delta_i$ . The red and yellow arcs represent different correct directions, respectively. To conclude, the correction of the safety filter is related to two factors: 1)  $d_{1,2}$ : the distance between two airplanes; 2)  $\angle(\phi_i - \beta_i)$ : the included angle between cruising direction and bearing of the other airplane. The behavior of the safety filter is fully captured by the explicit solution in the following theorem,

**Theorem 1.** *Considering a two-airplane system  $\mathcal{A} = \{A_1, A_2\}$  with dynamics in Eq. (2) and cruising controllers*

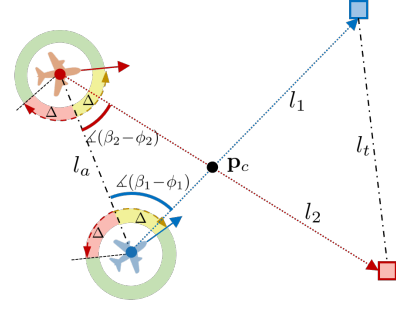


Fig. 4: Sketch of explicit solution for the safety filter.  $l_a$  is a line segment connecting  $\mathbf{x}_1$  and  $\mathbf{x}_2$ , while  $l_t$  connects  $\mathbf{T}_1$  and  $\mathbf{T}_2$ . As for  $i = 1, 2$ ,  $l_i$  connects  $\mathbf{x}_i$  and  $\mathbf{T}_i$ .  $\mathbf{p}_c$  is the intersection point of  $l_1$  and  $l_2$ .

in Eq.(4), the explicit solution to the safety filter of  $A_i$  in Eq.(5) is as follows,

$$\begin{aligned} \mathbf{u}_i &= v[\cos(\theta_i), \sin(\theta_i)]^T \\ \theta_i &= \angle(\tilde{\theta}_i) \\ \tilde{\theta}_i &= \begin{cases} \beta_i + \Delta \text{ or } \beta_i - \Delta, & \phi_i = \beta_i \\ \beta_i - \Delta, & \angle(\phi_i - \beta_i) \in (-\Delta, 0) \\ \beta_i + \Delta, & \angle(\phi_i - \beta_i) \in (0, \Delta) \\ \phi_i, & \text{otherwise} \end{cases} \end{aligned} \quad (6)$$

where  $\angle(\cdot)$  denotes the angular normalization operation defined in Eq. (1), and  $\Delta = \cos^{-1}\left(\min\left(1, \frac{\alpha h(x)}{4vd_{1,2}}\right)\right) \in [0, \frac{\pi}{2}]$ ,  $i, j = \{1, 2\}$  and  $i \neq j$ .

*Proof.* The proof is attached in Appendix B.

Note that both of  $\beta_i - \Delta$  and  $\beta_i + \Delta$  are feasible solutions when  $\phi_i = \theta_i$ . Herein, we assume  $A_i$  has a unique preferred direction, denoted by  $\lambda_i \in \{-1, 1\}$ , at  $\phi_i = \theta_i$ . Thus,  $\tilde{\theta}_i = \beta_i + \lambda_i \Delta$ ,  $i \in \{1, 2\}$ . The preferred direction plays a crucial role in the subsequent discussion on deadlock and livelock.

#### B. Blocking condition

Regarding the definition of blocking modes, zero relative angular velocity and activated safety filter are two necessary characteristics of blocking mode. Since  $\|\mathbf{x}_1 - \mathbf{x}_2\| \geq r \neq 0$ ,  $\omega = 0$  implies  $(\mathbf{v}_1 - \mathbf{v}_2)$  is parallel to  $(\mathbf{x}_1 - \mathbf{x}_2)$  or  $\mathbf{v}_1 = -\mathbf{v}_2$ . In terms of explicit solutions in Theorem 1, we can obtain a necessary and sufficient condition of blocking modes.

**Theorem 2** (Condition in the blocking mode). *Consider a two-airplane system  $\mathcal{A} = \{A_1, A_2\}$  in Eq. (2) in which each airplane is equipped with a nominal controller in Eq.(4) and a safety filter in Eq.(5). Supposing the system is in an encounter situation,*

- 1) *Both  $A_1$  and  $A_2$  have been in blocking if and only if  $\exists s \in \{-1, +1\}$ ,  $s\angle(\phi_1 - \beta_1) \in [0, \Delta)$  and  $-s\angle(\phi_2 - \beta_2) \in [0, \Delta)$ ;*
- 2) *Only  $A_1$  has been in blocking mode and  $A_2$  is in cruising mode if and only if  $\exists s \in \{-1, +1\}$ ,  $s\angle(\phi_1 - \beta_1) \in [0, \Delta)$  and  $\phi_2 = \angle(\beta_1 + s\Delta)$ ;*

*Proof.* The proof is attached in Appendix C.



Intuitively, the theorem implies that an airplane enters into blocking mode when the safety filters generate an avoiding direction symmetrically aligned with the heading direction of another airplane relative to the vertical centerline of  $l_a$ , continuously preventing it from bypassing. Particularly under condition 1), the safety filters of both airplanes generate symmetric avoiding directions. As shown in Fig. 4, when the  $\phi_1$  and  $\phi_2$  fall within the fan-shaped range of the same yellow/red color, the corrected direction of airplanes are symmetric, making both airplanes in blocking modes. In this case, we can see that the locations of target positions play a crucial role in determining the optimal bypassing direction. If two airplanes approach each other symmetrically in cruising mode, the blocking mode will be triggered inevitably. Consequently, we can deduce a sufficient condition of blocking modes about the symmetric placement of target points, which is formally stated in Corollary 1 using the geometric relationship in Fig. 4. In contrast to Theorem 2, this corollary facilitates advance detection of potential blocking modes.

**Corollary 1** (Condition leading to a blocking mode). *Considering a two-airplane system  $\mathcal{A} = \{A_1, A_2\}$  as described in Theorem 2 where each airplane is in cruising mode, and supposing the system has an encounter conflict, both airplanes will enter into the blocking modes if the placements of  $\mathbf{T}_1$  and  $\mathbf{T}_2$  make  $\angle(\phi_1 - \beta_1) = -\angle(\phi_2 - \beta_2)$  and  $\|\mathbf{x}_2 - \mathbf{p}_c\| = \|\mathbf{x}_1 - \mathbf{p}_c\|$ .*

*Proof.* The proof is attached in Appendix D.

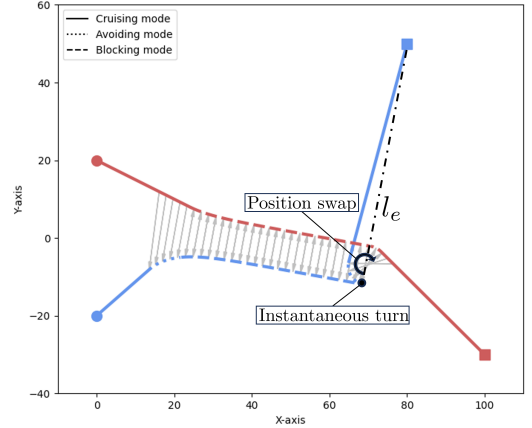
### C. Estimation of blocking duration

Having discussed how the safety filter causes blocking modes, we aim to estimate their duration and assess the resulting delays in task completion. To achieve this, we need to analyze airplane behavior during blocking modes and identify the conditions under which they end.

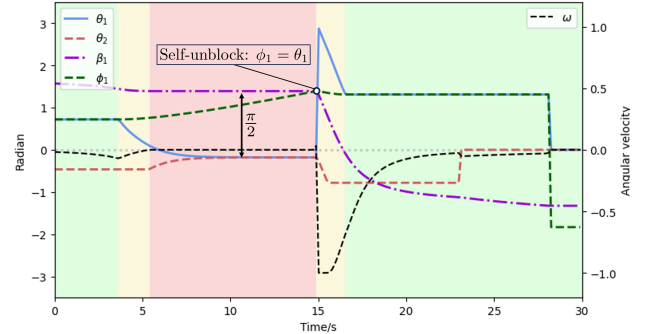
As shown in Theorem 2, the conditions for blocking modes depend on the  $\phi_i$ ,  $\beta_i$ , and  $\Delta_i$  for  $i \in \{1, 2\}$ . Fig. 5 shows the entire process of an encounter scenario where a blocking mode occurs and the corresponding curves of  $\phi_1$ ,  $\beta_1$ ,  $\Delta_1$ ,  $\theta_1$  and  $\omega$ . Because the solution  $\mathbf{x}$  to the system in (2) is continuous over time,  $\phi_i$ ,  $\beta_i$ , and  $\Delta_i$ , as continuous functions of  $\mathbf{x}$ , also evolve continuously. When an airplane enters a blocking mode,  $\omega = 0$  implies that  $\beta_i$  remains fixed, and  $\Delta_i$  remains fixed or converges to  $\frac{\pi}{2}$ , as shown in Fig. 5b. Consequently, breaking the blocking condition depends solely on the change of  $\phi_i$ . As demonstrated in Appendix E, once  $A_i$  enters the blocking mode,  $\phi_i$  eventually converges to  $\beta_i$ . Thus, the blocking mode is resolved by the position swap when the changes of  $\phi_1$  and  $\phi_2$  break the blocking condition in Theorem 2, as depicted in Fig. 5b. Based on this, we derive the following corollary about the self-unblock of blocking modes,

**Corollary 2** (Self-unblock condition). *Considering the system setting described in Theorem 2, once an airplane enters into blocking mode, blocking mode remains until for  $\exists i, j \in \{1, 2\}$  and  $i \neq j$  such that  $\phi_i = \beta_i$  and  $\phi_j \neq \beta_j$ .*

*Proof.* The proof is attached in Appendix E.



(a) Trajectories of two airplanes in blocking mode. Gray arrows represent the activation of safety filters.



(b) Curves of related variables. Light green, yellow, and red areas denote the cruising, avoiding, and blocking modes of  $A_1$ , respectively.

Fig. 5: The process of an encounter with a blocking mode.

Geometrically,  $\beta_i = \phi_i$  implies  $\mathbf{x}_i$ ,  $\mathbf{x}_j$  and  $\mathbf{T}_i$  are collinear, as depicted by  $l_e$  in Fig. 5b. After the moment, the blocking will be broken. In terms of this characteristic, we can calculate the bounds of the expected blocking time  $T \in [T_{lb}, T_{ub}]$  based on the simple geometric relationship, where

$$\begin{aligned} T_{lb} &= \frac{\min(\|\mathbf{x}_1 - \mathbf{T}_1\| \cos(\beta_1 - \phi_1), \|\mathbf{x}_2 - \mathbf{T}_2\| \cos(\beta_2 - \phi_2))}{v} \\ T_{ub} &= T_{lb} + \frac{\|\mathbf{x}_1 - \mathbf{x}_2\| - r}{2v}. \end{aligned} \quad (7)$$

The rigorous derivation is attached in Appendix F. Notably, once the blocking mode is resolved, the airplane makes an instantaneous turn shown in Fig. 5b, an unrealistic behavior caused by the simplifications of the airplane model in Eq. (2).

### D. Deadlock and livelock phenomenon

Besides the finite-time blocking modes, deadlock and livelock phenomena can occur under specific conditions. Deadlock arises when airplanes cannot indefinitely satisfy the condition in Corollary 2. Specifically, deadlock occurs during blocking mode when two additional conditions are met: 1) the relative position of airplanes is negatively proportional to their target displacement, expressed as  $\mathbf{x}_1 - \mathbf{x}_2 = -k(\mathbf{T}_1 - \mathbf{T}_2)$ , where  $k > 0$ ; and 2) The preferred actions of airplanes are opposite, so  $\lambda_1 = -\lambda_2$ . Because of the first condition, both airplanes reach the line  $l_t$  in Fig. 4 simultaneously, causing  $\mathbf{x}_1$ ,  $\mathbf{x}_2$ ,  $\mathbf{T}_1$  and  $\mathbf{T}_2$  to become collinear, as shown in Fig. 6a. At this moment, the second condition causes both airplanes to simultaneously switch avoiding directions between  $\beta_i - \frac{\pi}{2}$  and

$\beta_i + \frac{\pi}{2}$  while remaining symmetric to each other. As a result, the airplanes will stall along the line  $l_t$  at a separation distance of  $d_{1,2} = r$ . If the airplanes have the same preferred directions, they are still able to resolve the blocking mode. However, when the preferred directions of two airplanes are identical, the livelock phenomenon could occur if both airplanes share the same target position. As depicted in Fig. 6b, airplanes fly around the target endlessly without reaching it, when  $\mathbf{T}_1 = \mathbf{T}_2$  and  $\lambda_1 = \lambda_2$ . In this situation, rotation maneuvers are defective in resolving conflicts. However, sharing the same target is a special terminal encounter commonly occurring near airports, which does not meet the definition of the encounter situation considered in this paper. Therefore, encounter situations defined in Def. 1 have a risk of blocking and deadlock phenomenon but not the livelock phenomenon. In the next section, we introduce a resolution strategy for blocking modes in encounter situations, which incidentally eliminates deadlock.

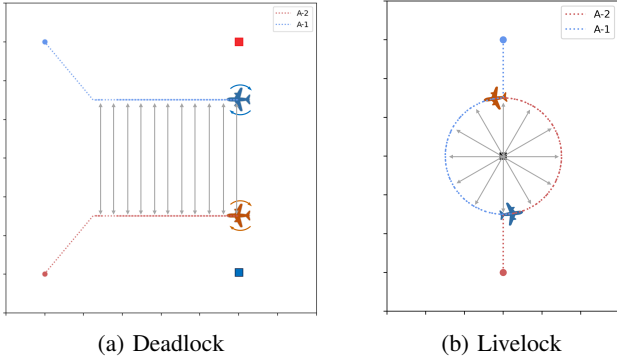


Fig. 6: Deadlock and livelock phenomenon in simulation.

#### IV. BLOCKING RESOLUTION FRAMEWORK

In this section, we develop a novel intention-aware unblocking framework facilitated by adaptive priority. We first propose an unblocking maneuver based on adaptive priority, assuming that both agents know precisely each other's intentions, i.e., their target points. Then, we also design an interactive maneuver that does not require this knowledge, where airplanes can reveal their intentions and estimate the intention of the other without relying on direct communication. This unblocking framework is illustrated in Algorithm 1.

##### A. Unblocking maneuver

Eq. (7) reveals that the duration of blocking and deadlock largely depends on the positions of the target points. According to Corollary 2, an efficient approach to reduce this duration is to place a temporary target to trigger the self-unblock condition, named the *unblocking maneuver*, specifically, setting the executed target  $\hat{\mathbf{T}}_i$  of  $A_i$  to the current position  $\mathbf{x}_j$  of  $A_j$ , expressed as  $\hat{\mathbf{T}}_i \leftarrow \mathbf{x}_j$ . However, if both airplanes simultaneously initiate unblocking maneuvers, a new blocking mode will occur. Thus, priority must be assigned to the airplanes to prevent this. We develop an adaptive priority system to mitigate the inefficiency of the fixed-priority method, such as the right-hand rule, by selecting the decision with the shortest time duration among three options: maintaining

---

##### Algorithm 1: Blocking resolution strategy for $A_i$

---

```

1 Input:  $\mathbf{x}_i, \mathbf{x}_j, \mathbf{T}_i, \theta_j, \omega$ ;
2 Output:  $\mathbf{u}_i$ ;
3 Initial:  $\hat{\mathbf{T}}_i \leftarrow \mathbf{T}_i, \tilde{\mathbf{T}}_j \leftarrow \text{None}, \mathcal{T} \leftarrow \emptyset, F_i \leftarrow \text{False}$ ;
4 if  $\mathbf{x}_i \neq \mathbf{T}_i$  then
5    $\tilde{\mathbf{u}}_i \leftarrow \mathcal{N}(\mathbf{x}_i, \hat{\mathbf{T}}_i)$  in (4);
6    $\mathbf{u}_i \leftarrow \mathcal{F}(\mathbf{x}_i, \mathbf{x}_j, \tilde{\mathbf{u}}_i)$  in (5);
7   if  $\mathbf{u}_i \neq \tilde{\mathbf{u}}_i$  and  $\omega = 0$  then
8     /* $A_i$  is in blocking.*/
9     if  $\tilde{\mathbf{T}}_j = \text{None}$  then
10      /*Interactive maneuver*/
11       $\mathbf{u}_i \leftarrow \mathbf{u}_i + \Delta \mathbf{u}$ ;
12       $F_i \leftarrow \text{True}$ ;
13    else
14      /*Unblocking maneuver*/
15      if  $\text{Priority}(\mathbf{x}_i, \mathbf{x}_j, \mathbf{T}_i, \tilde{\mathbf{T}}_j) = \text{True}$  then
16        /*Set temporary target*/
17         $\hat{\mathbf{T}}_i \leftarrow \mathbf{x}_j$ ;
18    if  $\mathbf{x}_i = \hat{\mathbf{T}}_i$  and  $\hat{\mathbf{T}}_i \neq \mathbf{T}_i$  then
19      /*Recover original target*/
20       $\hat{\mathbf{T}}_i \leftarrow \mathbf{T}_i$ ;
21    if  $F_i = \text{True}$  and  $\mathbf{u}_i = \tilde{\mathbf{u}}_i$  then
22      /*Estimate intention*/
23       $\tilde{\mathbf{T}}_j, \mathcal{T} \leftarrow \text{Estimate}(\mathcal{T}, \mathbf{x}_j, \theta_j)$ ;
24       $F_i \leftarrow \text{False}$ ;

```

---

the current blocking mode, unblocking by  $A_1$ , or unblocking by  $A_2$ . The estimation of time duration for these options is introduced in Appendix G. If all airplanes use the same assessment method, they will independently reach a common agreement on the priority order without communication. This function is encoded in *Priority()* function in Algorithm 1.

##### B. Interactive maneuver for intention estimate

To estimate the target points of another airplane without communication, the ego agent can provoke the other airplane to reveal its intentions actively. Since an airplane naturally heads toward its target when its safety filter is inactive, we designed an *interactive maneuver* where the ego agent temporarily moves away from the opponent until the opponent's safety filter deactivates. Specifically, when  $A_i$  adopts an interactive maneuver, the input  $\mathbf{u}_i$  generated by the safety filter is modified by adding  $\Delta \mathbf{u} = k(\mathbf{x}_i - \mathbf{x}_j)$ , to drive  $A_i$  away from  $A_j$ , where  $k$  is a positive constant. Regardless of which airplane takes this maneuver, both airplanes can revert to their cruising modes and reveal their intended directions. Therefore, each agent can accurately estimate the other's intention and also allow the other to estimate its own intention.

When the two-airplane model  $\mathcal{A}$  is deterministic, i.e., not incorporating the stochastic noise, observing two different cruising angles at different locations is sufficient for intention estimation. Specifically,  $\mathcal{T}$  in Algorithm 1 denotes the collection of cruising angles and the recorded position of the

other airplane. Once  $\mathcal{T}$  of  $A_i$  has two cruising angles, the targets of the other airplane can be estimated, denoted as  $\tilde{\mathbf{T}}_j$ . This function is implemented in *Estimate()* of Algorithm 1. When incorporating the stochastic noise, more information is needed to improve the estimation precision. Mutual intention estimation can be achieved whether one or both agents initiate interactive maneuvers.

## V. SIMULATION EXPERIMENTS

This section demonstrates the efficacy of the proposed resolution strategy on both the simple model in (2) and a more realistic model.

### A. Simulation for the resolution strategy

Fig. 7 illustrates the unblocking process using the resolution strategy introduced in Sec. IV. Airplanes  $A_1$  and  $A_2$  are initially positioned at  $(0, -30)$  and  $(0, 30)$ , respectively, and are directed towards their target destinations at  $\mathbf{T}_1 = (80, 50)$  and  $\mathbf{T}_2 = (100, -30)$ . The system parameters are set to  $v = 5$ ,  $r = 30$ , and  $\alpha = 3$ . Firstly, a blocking mode is detected during an encounter situation, prompting the two airplanes to initiate interactive maneuvers. Secondly, airplanes reveal their intentions through interactive maneuvers, allowing mutual estimation of each other's target points. Using the estimated target points,  $A_1$  is selected to conduct unblocking maneuvers through time estimation.  $\mathbf{T}_1$  is replaced by a temporal target point that can break the ongoing blocking mode and make airplanes return to an avoiding mode. When  $A_1$  reaches the temporal target, the encounter conflict is resolved at this moment such that  $A_1$  heads towards the original target. Simulation in Fig. 7 demonstrates the efficacy of the proposed strategy in Algorithm 1.

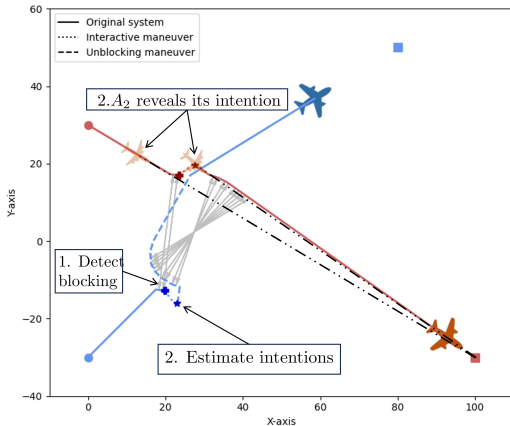


Fig. 7: Blocking resolution process using Algorithm 1. Plus markers represent the moment when the blocking mode is detected; star markers represent the moment of successful intention estimation. Gray arrows represent the activation of safety filters. The intersection point of two black dotted dashed lines is the estimated target of  $A_2$  from  $A_1$ .

### B. Monte Carlo simulation for adaptive priority

To evaluate the proposed unblocking maneuver based on the adaptive priority, we test the strategy in randomly generated

encounter scenarios. Specifically, we fix the initial points of airplanes and randomly select their target points within diagonal regions. For instance,  $A_1$  is initialized at  $(0, 15)$  with target points sampled in the rectangle region defined by  $T_x \in [0, 100]$  and  $T_y \in [-100, 0]$ ; Conversely,  $A_2$  is initialized at  $(0, -15)$  with target points sampled over the region where  $T_x \in [0, 100]$  and  $T_y \in [0, 100]$ . In terms of Theorem 2,  $A_1$  and  $A_2$  are in blocking mode initially. This configuration with a scale of 100 is termed as *region\_100*. Likewise, we adopt two additional sampling configurations with larger scales, *region\_200* and *region\_300*, leading to longer journeys in encounter situations. For each configuration, 100 randomized encounter scenarios are generated. For sampled scenarios, we measure the duration of task accomplishment using three strategies: maintaining blocking, unblocking strategy with fixed priority, and adaptive priority. Fig. 8 compares the average additional time incurred by these three strategies relative to the minimal unblocking behavior. Compared with maintaining the blocking, the unblocking strategy significantly reduces time and the adaptive-priority strategy outperforms the fixed-priority strategy. Meanwhile, this advantage is more obvious for longer journeys. There is no doubt that the adaptive priority strategy statistically improves performance.

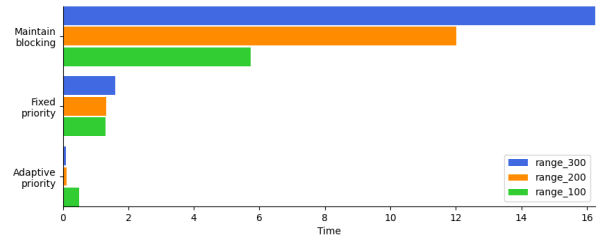


Fig. 8: Comparison of average additional time for maintaining blocking, unblocking with fixed priority, and unblocking with adaptive priority in randomly generated encounter scenarios with different scales.

### C. Simulation on unicycle model

As previously mentioned, the simplified model in Eq. (2) can generate instantaneous turns that are unrealistic in real airplanes. To verify the applicability of analytical results to more realistic systems, we consider a unicycle model with constant speed for each airplane. The blocking phenomenon is also observed in unicycle models, as shown in Fig. 9a. We then apply the strategy developed for the simple model (2) to the unicycle model. As shown in Fig. 9b, the blocking phenomenon is successfully resolved, demonstrating the proposed resolution strategy is effective for the unicycle system as well. To conclude, both the analytical results and the resolution strategy are applicable to more realistic unicycle models.

## VI. CONCLUSION

Beyond the widely studied deadlock, this paper investigated the finite-time blocking phenomenon observed in a two-airplane encounter scenario. We reproduced and analyzed the blocking behavior using a simplified model of a two-airplane system. Analytical results revealed that blocking occurs when

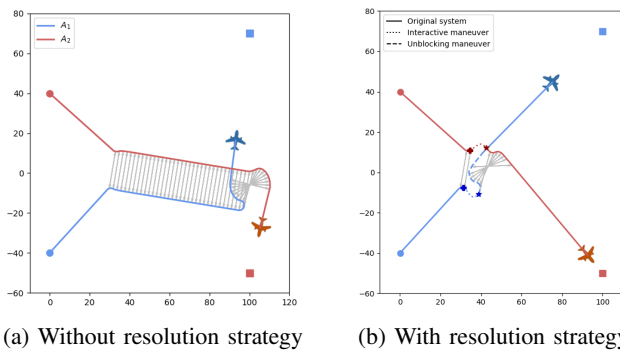


Fig. 9: Comparison of the blocking phenomenon with and without the resolution strategy using unicycle airplane models.

the safety filters generate symmetric avoidance directions following the optimality principle. Instead of relying on external factors like communications and central coordinators, this paper proposed an efficient and guaranteed resolution strategy based on intention awareness. Therefore, this strategy can serve as a backup even when communication fails in increasingly complex airspace. Although blocking behavior manifests differently, finite-time pathological phenomena likely exist in other multi-agent systems where agents are equipped with similar or identical controllers, such as the interaction between autonomous vehicles. Therefore, the results in this paper offer insights across various applications. As this paper is the first attempt to analyze the finite-time blocking phenomenon in airplane systems, we focus solely on a two-airplane encounter scenario using a simplified model. Further work is needed to account for more complex dynamics and realistic uncertainty in multiple-airplane encounter scenarios.

## REFERENCES

- [1] K. Namuduri, U.-C. Fiebig, D. W. Matolak, I. Guvenc, K. Hari, and H.-L. Määtänen, “Advanced air mobility: Research directions for communications, navigation, and surveillance,” *IEEE Vehicular Technology Magazine*, vol. 17, no. 4, pp. 65–73, 2022.
- [2] M. J. Kochenderfer, L. P. Espindle, J. K. Kuchar, and J. D. Griffith, “A comprehensive aircraft encounter model of the national airspace system,” *Lincoln Laboratory Journal*, vol. 17, no. 2, pp. 41–53, 2008.
- [3] C. Tomlin, G. Pappas, and S. Sastry, “Conflict resolution for air traffic management: a study in multi-agent hybrid systems,” *IEEE Transactions on Automatic Control*, vol. 43, no. 4, pp. 509–521, 1998.
- [4] S. Bharadwaj, S. Carr, N. Neogi, and U. Topcu, “Decentralized control synthesis for air traffic management in urban air mobility,” *IEEE Transactions on Control of Network Systems*, vol. 8, no. 2, pp. 598–608, 2021.
- [5] E. O. for Civil Aviation Equipment (EUROCAE), “Operational services & environment definition (osed) for detect & avoid in very low-level operations,” 2020.
- [6] S. Stroeve, C.-J. Villanueva-Cañizares, and G. Dean, “The critical impact of remote pilot modelling in evaluation of detect-and-avoid systems explained for acas xu,” *European Journal of Transport and Infrastructure Research*, vol. 24, p. 1–17, Nov. 2024.
- [7] A. Abate, A. D’Innocenzo, M. D. Di Benedetto, and S. Sastry, “Understanding deadlock and livelock behaviors in hybrid control systems,” *Nonlinear Analysis: Hybrid Systems*, vol. 3, no. 2, pp. 150–162, 2009.
- [8] M. Jankovic, M. Santillo, and Y. Wang, “Multiagent systems with cbf-based controllers: Collision avoidance and liveness from instability,” *IEEE Transactions on Control Systems Technology*, 2023.
- [9] J. Grover, C. Liu, and K. Sycara, “The before, during, and after of multi-robot deadlock,” *The International Journal of Robotics Research*, vol. 42, no. 6, pp. 317–336, 2023.
- [10] Y. Chen, M. Guo, and Z. Li, “Deadlock resolution and recursive feasibility in mpc-based multi-robot trajectory generation,” *IEEE Transactions on Automatic Control*, pp. 1–16, 2024.
- [11] L. Wang, A. D. Ames, and M. Egerstedt, “Safety barrier certificates for collisions-free multirobot systems,” *IEEE Transactions on Robotics*, vol. 33, no. 3, pp. 661–674, 2017.
- [12] Y. Chen, C. Wang, M. Guo, and Z. Li, “Multi-robot trajectory planning with feasibility guarantee and deadlock resolution: An obstacle-dense environment,” *IEEE Robotics and Automation Letters*, vol. 8, no. 4, pp. 2197–2204, 2023.
- [13] Z. Ouyang, J. Liu, H. Lu, and W. Zhang, “Fast decentralized multi-agent collision avoidance based on safe-reachable sets,” in *2023 62nd IEEE Conference on Decision and Control (CDC)*, pp. 8369–8375, 2023.
- [14] M. F. Reis, A. P. Aguiar, and P. Tabuada, “Control barrier function-based quadratic programs introduce undesirable asymptotically stable equilibria,” *IEEE Control Systems Letters*, vol. 5, no. 2, pp. 731–736, 2020.
- [15] J. Grover, C. Liu, and K. Sycara, “Why does symmetry cause deadlocks?,” *IFAC-PapersOnLine*, vol. 53, no. 2, pp. 9746–9753, 2020.
- [16] A. Tanenbaum, *Modern operating systems*. Pearson Education, Inc., 2009.
- [17] A. Mannucci, L. Pallottino, and F. Pecora, “On provably safe and live multirobot coordination with online goal posting,” *IEEE Transactions on Robotics*, vol. 37, no. 6, pp. 1973–1991, 2021.
- [18] P. Yu and D. V. Dimarogonas, “Distributed motion coordination for multirobot systems under ltl specifications,” *IEEE Transactions on Robotics*, vol. 38, no. 2, pp. 1047–1062, 2021.
- [19] M. Chen, J. C. Shih, and C. J. Tomlin, “Multi-vehicle collision avoidance via hamilton-jacobi reachability and mixed integer programming,” in *2016 IEEE 55th Conference on Decision and Control (CDC)*, pp. 1695–1700, 2016.
- [20] W. Hönig, J. A. Preiss, T. K. S. Kumar, G. S. Sukhatme, and N. Ayanian, “Trajectory planning for quadrotor swarms,” *IEEE Transactions on Robotics*, vol. 34, no. 4, pp. 856–869, 2018.
- [21] B. Weng, H. Chen, and W. Zhang, “On the convergence of multi-robot constrained navigation: A parametric control lyapunov function approach,” in *2022 International Conference on Robotics and Automation (ICRA)*, pp. 4972–4978, IEEE, 2022.
- [22] S. H. Arul and D. Manocha, “V-rvo: Decentralized multi-agent collision avoidance using voronoi diagrams and reciprocal velocity obstacles,” in *2021 IEEE/RSJ International Conference on Intelligent Robots and Systems (IROS)*, pp. 8097–8104, 2021.
- [23] S. E. S. A. R. Project, *European ATM master plan – Digitalising Europe’s aviation infrastructure – Executive view*. 2020.
- [24] D. Zhou, Z. Wang, S. Bandyopadhyay, and M. Schwager, “Fast, on-line collision avoidance for dynamic vehicles using buffered voronoi cells,” *IEEE Robotics and Automation Letters*, vol. 2, no. 2, pp. 1047–1054, 2017.
- [25] A. Pierson, W. Schwarting, S. Karaman, and D. Rus, “Weighted buffered voronoi cells for distributed semi-cooperative behavior,” in *2020 IEEE international conference on robotics and automation (ICRA)*, pp. 5611–5617, IEEE, 2020.
- [26] A. Platzer and E. M. Clarke, “Formal verification of curved flight collision avoidance maneuvers: A case study,” in *International Symposium on Formal Methods*, pp. 547–562, Springer, 2009.
- [27] M. Čáp, J. Gregoire, and E. Frazzoli, “Provably safe and deadlock-free execution of multi-robot plans under delaying disturbances,” in *2016 IEEE/RSJ International Conference on Intelligent Robots and Systems (IROS)*, pp. 5113–5118, IEEE, 2016.
- [28] Z. Sun, H. Garcia de Marina, B. D. Anderson, and C. Yu, “Collaborative target-tracking control using multiple fixed-wing unmanned aerial vehicles with constant speeds,” *Journal of Guidance, Control, and Dynamics*, vol. 44, no. 2, pp. 238–250, 2021.
- [29] K. P. Wabersich, A. J. Taylor, J. J. Choi, K. Sreenath, C. J. Tomlin, A. D. Ames, and M. N. Zeilinger, “Data-driven safety filters: Hamilton-jacobi reachability, control barrier functions, and predictive methods for uncertain systems,” *IEEE Control Systems Magazine*, vol. 43, no. 5, pp. 137–177, 2023.
- [30] M. Jankovic and M. Santillo, “Collision avoidance and liveness of multi-agent systems with cbf-based controllers,” in *2021 60th IEEE Conference on Decision and Control (CDC)*, pp. 6822–6828, 2021.
- [31] A. D. Ames, S. Coogan, M. Egerstedt, G. Notomista, K. Sreenath, and P. Tabuada, “Control barrier functions: Theory and applications,” in *2019 18th European control conference (ECC)*, pp. 3420–3431, IEEE, 2019.



## APPENDIX

## A. Decentralized CBF Condition

In this section, we describe how the CBF condition in (5b) is designed to ensure the safety of the system in (2) in a decentralized manner. We begin by defining the safety property. The collision-free safety formally implies the system states to stay in  $\mathcal{C}$  both in the current and future, which can be represented by the forward invariance property as follows,

**Definition 4** (Forward Invariance [31]). *A set  $\mathcal{C} \subset \mathbb{X}$  is forward invariant if  $\forall x_0 \in \mathcal{C}$ ,  $\mathbf{x}(t) \in \mathcal{C}$  for  $\mathbf{x}(0) = x_0$  and all  $t > 0$ . The system  $\dot{\mathbf{x}} = f(\mathbf{x})$  is safe to the set  $\mathcal{C}$  if the set  $\mathcal{C}$  is forward invariant.*

The forward invariance of a system for a given safe set  $\mathcal{C}$  can be achieved using control barrier functions (CBF) [31].

**Definition 5** (Control barrier function, CBF). *Let  $\mathcal{C} \subset \mathbb{R}^n$  be the super level set of a continuously differentiable function  $h : \mathbb{R}^n \rightarrow \mathbb{R}$ , then  $h$  is a valid control barrier function (CBF) if there exists a continuous function  $\alpha : \mathbb{R} \rightarrow \mathbb{R}$  such that for all  $x \in \mathbb{R}^2$ :*

$$\alpha(h(\mathbf{x})) + \frac{\partial h(\mathbf{x})}{\partial t} \geq 0.$$

where  $\alpha$  is strictly monotonically increasing and  $\alpha(0) = 0$ .

In this paper, we use a linear function  $\alpha(h(x)) = \alpha h(x)$ ,  $\alpha \in \mathbb{R}_{>0}$  for simplicity. From the definition, we can directly derive the following CBF conditions for (3),

$$\alpha h(\mathbf{x}) + 2(\mathbf{x}_i - \mathbf{x}_j)^T (\mathbf{u}_i - \mathbf{u}_j) \geq 0,$$

for  $i \neq j$  and  $i, j \in \{1, 2\}$ . Note that the above condition relies on the control inputs of both airplanes, which implies a centralized control manner. To obtain decentralized conditions, more conservative CBFs are designed in [9], [11], [30], based on the assumption for predefined responsibility assignment of each agent. Without the loss of generality, we assume both airplanes take half responsibility for avoiding collision. Thus, we use the following decentralized CBF condition

$$\frac{\alpha}{2} h(\mathbf{x}) + 2(\mathbf{x}_i - \mathbf{x}_j)^T \mathbf{u}_i \geq 0. \quad (8)$$

## B. Proof of Theorem 1

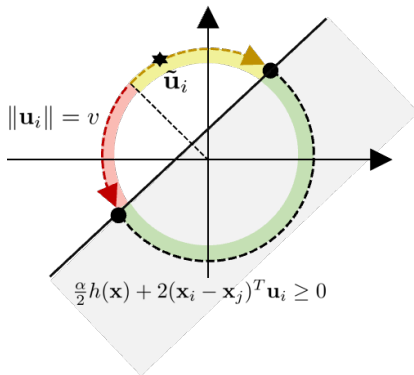


Fig. 10: Geometric interpretation of the safety filter in Eq. (5).

Fig. 10 provides a geometric interpretation of the original optimization problem in Eq. (5). Considering the inequality constraint in Eq. (5b) and equality constraint in Eq. (5c), the

admissible solution set refers to the block dashed circular arc. Considering the objective of minimizing the absolute difference between the nominal input and the final input, the optimal solution is the nominal input if the nominal input is in the admissible set. Otherwise, the optimal solution is the nearest admissible solution from the nominal solution, i.e., the nearest black circular point from the nominal solution represented by the star marker in Fig. 10. To numerically analyze the optimization problem in Eq. (5), it is better to use the parametric approach of  $\mathbf{u}_i = v[\cos(\theta_i), \sin(\theta_i)]^T$  and  $\tilde{\mathbf{u}}_i = v[\cos(\phi_i), \sin(\phi_i)]^T$ , which implicitly satisfy the norm constraint in Eq. (5c). The origin objective in Eq. (5a) can be transformed into the following formula,

$$\begin{aligned} \frac{1}{2} \|\mathbf{u}_i - \tilde{\mathbf{u}}_i\|^2 &= \frac{1}{2} \left\| \begin{bmatrix} \cos(\theta_i) - \cos(\phi_i) \\ \sin(\theta_i) - \sin(\phi_i) \end{bmatrix} \right\|^2 \\ &= 1 - \cos(\theta_i - \phi_i) \end{aligned}$$

The CBF condition in Eq. (5b) can be derived into,

$$\begin{aligned} \frac{\alpha}{2} h(\mathbf{x}) - 2v \|\mathbf{x}_i - \mathbf{x}_j\| \begin{bmatrix} \cos(\beta_i) \\ \sin(\beta_i) \end{bmatrix}^T \begin{bmatrix} \cos(\theta_i) \\ \sin(\theta_i) \end{bmatrix} &\geq 0 \\ \Rightarrow \cos(\theta_i - \beta_i) &\leq \frac{\alpha h(\mathbf{x})}{4v \|\mathbf{x}_1 - \mathbf{x}_2\|} \end{aligned}$$

Let  $L(\mathbf{x})$  denote the right-side term of the inequality function. Since  $\alpha$  and  $v$  are positive constant numbers,  $L(\mathbf{x}) \geq 0$  if the current state is in the safe set. Given the above derivation, the optimization problem in Eq. (5) for  $h(\mathbf{x})$  in Eq. (3) can be transformed into the formulation from the angular perspective,

$$\begin{aligned} \min_{\theta_i \in (-\pi, \pi]} & 1 - \cos(\theta_i - \phi_i) \\ \text{s.t.} & \cos(\theta_i - \beta_i) \leq L(\mathbf{x}) \end{aligned} \quad (9)$$

Without the loss of generality, we assume  $\beta_i, \theta_i, \phi_i \in (-\pi, \pi]$ . With the angular normalization operator  $\angle(\cdot) \in (-\pi, \pi]$ , the optimization can be further transformed into,

$$\begin{aligned} \min_{\theta_i \in (-\pi, \pi]} & |\angle(\theta_i - \phi_i)| \\ \text{s.t.} & |\angle(\theta_i - \beta_i)| \in [\Delta(\mathbf{x}), \pi] \end{aligned} \quad (10)$$

where  $\Delta(\mathbf{x}) = \cos^{-1}(\min(1, L(\mathbf{x}))) \in [0, \frac{\pi}{2}]$ . With the reformulated optimization problem from angular perspective, the explicit solution can be easily obtained in a form of piecewise functions, as shown in Eq. (6).

## C. Proof of Theorem 2

**Sufficiency:** As for condition (1), since  $s\angle(\phi_1 - \beta_1) \in [0, \Delta)$  and  $-s\angle(\phi_2 - \beta_2) \in [0, \Delta)$ , the heading directions corrected by safety filters are  $\theta_1 = \angle(\beta_1 + s\Delta)$  and  $\theta_2 = \angle(\beta_2 - s\Delta)$ . Since  $\angle(\beta_1 - \beta_2) = \pi$ ,

$$\begin{aligned} \mathbf{v}_2 - \mathbf{v}_1 &= \begin{bmatrix} \cos(\beta_1 + s\Delta) - \cos(\beta_2 - s\Delta) \\ \sin(\beta_1 + s\Delta) - \sin(\beta_2 - s\Delta) \end{bmatrix} \\ &= 2\cos(\Delta) \begin{bmatrix} \cos(\beta_1) \\ \sin(\beta_1) \end{bmatrix} \\ &= 2 \frac{\cos(\Delta)}{d_{1,2}} (\mathbf{x}_2 - \mathbf{x}_1) \end{aligned}$$

Thus,  $(\mathbf{v}_2 - \mathbf{v}_1)$  is collinear to  $(\mathbf{x}_2 - \mathbf{x}_1)$  such that  $\omega = 0$ . Therefore,  $s\angle(\phi_1 - \beta_1) \in [0, \Delta)$  and  $-s\angle(\phi_2 - \beta_2) \in [0, \Delta)$  is a sufficient condition for both airplanes in blocking mode. As for condition (2),  $s\angle(\phi_1 - \beta_1) \in [0, \Delta)$  implies that  $\theta_1 =$

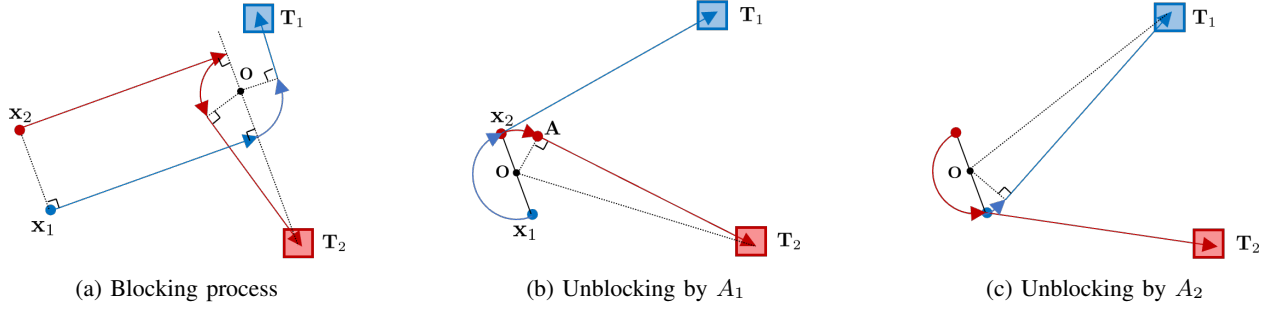


Fig. 11: Time assessment of three options.

$\angle(\beta_1 + s\Delta)$ . Given  $\phi_2 = \angle(\beta_1 \pm \Delta)$ ,  $\mathbf{v}_1 - \mathbf{v}_2 = 0$  such that  $\omega = 0$ . In addition, since  $\angle(\beta_1 - \beta_2) = \pi$ ,  $|\angle(\phi_2 - \beta_2)| \notin [0, \Delta)$ , which means  $A_2$  is in cruising mode. Therefore, the sufficiency of condition (2) is verified.

**Necessity:** Suppose  $A_1$  is in blocking mode such that  $\theta_1 = \angle(\beta_1 + s\Delta)$ . To make  $\omega_1 = 0$ , the following equality should be satisfied,

$$\begin{aligned} & (\mathbf{x}_2 - \mathbf{x}_1) \times (\mathbf{v}_2 - \mathbf{v}_1) \\ &= (\mathbf{x}_2 - \mathbf{x}_1) \times \mathbf{v}_2 - (\mathbf{x}_2 - \mathbf{x}_1) \times \mathbf{v}_1 \\ &= v \|\mathbf{x}_2 - \mathbf{x}_1\| \sin(\beta_1 - \theta_2) \vec{\mathbf{n}} - \|\mathbf{x}_2 - v\mathbf{x}_1\| \sin(\beta_1 - \theta_1) \vec{\mathbf{n}} \\ &= 0 \end{aligned}$$

where  $\vec{\mathbf{n}}$  denotes a unit vector perpendicular to the horizontal plane. Therefore,  $\sin(\beta_1 - \theta_2) = \sin(\beta_1 - \theta_1)$  to ensure  $\omega = 0$ . Given  $\theta_1 = \angle(\beta_1 + s\Delta)$  and  $\angle(\beta_1 - \beta_2) = \pi$ ,  $\sin(\beta_1 - \theta_2) = \sin(\beta_1 - \theta_1) = \sin(-s\Delta)$ . Therefore,  $\theta_2 = \angle(\beta_1 + s\Delta)$  or  $\theta_2 = \angle(\beta_1 - \pi - s\Delta) = \angle(\beta_2 - s\Delta)$ .

- 1) Suppose  $A_2$  is in blocking mode such that  $\|\angle(\phi_2 - \beta_2)\| \in [0, \Delta)$ . To make  $\omega = 0$ ,  $\theta_2 = \angle(\beta_2 - s\Delta)$  such that  $-s\angle(\phi_2 - \beta_2) \in [0, \Delta)$ .
- 2) Suppose  $A_2$  is not in blocking mode such that  $\|\angle(\phi_2 - \beta_2)\| \notin [0, \Delta)$ . To make  $\omega = 0$ ,  $\theta_2 = \angle(\beta_1 + s\Delta) = \theta_1$  such that  $\phi_2 = \angle(\beta_1 + s\Delta)$ .

Therefore, the necessity of conditions (1) and (2) is also verified.

#### D. Proof of Corollary 1

Under the conditions  $\angle(\phi_1 - \beta_1) = -\angle(\phi_2 - \beta_2)$  and  $\|\mathbf{x}_2 - \mathbf{p}_c\| = \|\mathbf{x}_1 - \mathbf{p}_c\|$ , the two airplanes in cruising mode approach the encounter point  $\mathbf{p}_c$  symmetrically with respect to their vertical midline. In this situation, they will activate their safety filters at the same time. Subsequently, they must enter the blocking mode because their cruising angles fall into the correction region on the same side; that is,  $\exists s \in \{-1, +1\}$ ,  $s\angle(\phi_1 - \beta_1) \in [0, \Delta)$  and  $-s\angle(\phi_2 - \beta_2) \in [0, \Delta)$ .

#### E. Proof of Corollary 2

Without the loss of generality, assume  $A_1$  is in blocking mode such that  $\|\beta_1 - \phi_1\| \in [0, \Delta)$  and  $\omega = 0$ . Since  $\omega = 0$ ,  $\frac{d}{dt} \left( \frac{\mathbf{x}_2 - \mathbf{x}_1}{\|\mathbf{x}_2 - \mathbf{x}_1\|} \right) = 0$ . Given  $\cos(\beta_1 - \phi_1) = \frac{(\mathbf{x}_2 - \mathbf{x}_1)^T (\mathbf{T}_1 - \mathbf{x}_1)}{\|\mathbf{x}_2 - \mathbf{x}_1\| \|\mathbf{T}_1 - \mathbf{x}_1\|}$ ,

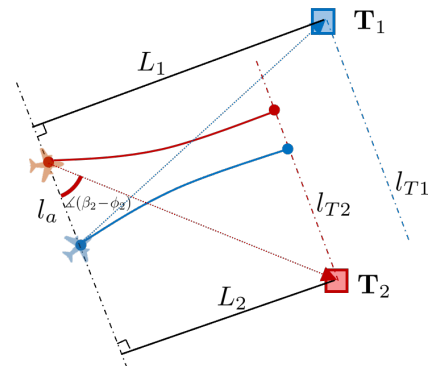
the derivative of  $\cos(\beta_1 - \phi_1)$  with respect to  $t$  is calculated as follows,

$$\begin{aligned} & \frac{d}{dt} \cos(\beta_1 - \phi_1) \\ &= \frac{d}{dt} \left( \frac{\mathbf{x}_2 - \mathbf{x}_1}{\|\mathbf{x}_2 - \mathbf{x}_1\|} \right)^T \frac{\mathbf{T}_1 - \mathbf{x}_1}{\|\mathbf{T}_1 - \mathbf{x}_1\|} + \frac{(\mathbf{x}_2 - \mathbf{x}_1)^T}{\|\mathbf{x}_2 - \mathbf{x}_1\|} \frac{d}{dt} \left( \frac{\mathbf{T}_1 - \mathbf{x}_1}{\|\mathbf{T}_1 - \mathbf{x}_1\|} \right) \\ &= \frac{(\mathbf{x}_2 - \mathbf{x}_1)^T}{\|\mathbf{x}_2 - \mathbf{x}_1\|} \cdot \frac{-\mathbf{u}_1 \|\mathbf{T}_1 - \mathbf{x}_1\|^2 + (\mathbf{T}_1 - \mathbf{x}_1)(\mathbf{T}_1 - \mathbf{x}_1)^T \mathbf{u}_1}{\|\mathbf{T}_1 - \mathbf{x}_1\|^3} \\ &= \frac{-v \cos(\beta_1 - \theta_1) + v \cos(\beta_1 - \phi_1) \cos(\phi_1 - \theta_1)}{\|\mathbf{T}_1 - \mathbf{x}_1\|} \\ &= \frac{v \sin(\beta_1 - \phi_1) \sin(\phi_1 - \theta_1)}{\|\mathbf{T}_1 - \mathbf{x}_1\|}. \end{aligned} \quad (11)$$

The above derivation used following two formulas:  $\frac{d}{dt} (\mathbf{a}^T \mathbf{b}) = \left( \frac{d}{dt} \mathbf{a} \right)^T \mathbf{b} + \mathbf{a}^T \left( \frac{d}{dt} \mathbf{b} \right)$  and  $\frac{d}{dt} \left( \frac{1}{\|\mathbf{b}\|} \right) = -\frac{\mathbf{b}^T}{\|\mathbf{b}\|^3} \frac{d}{dt} (\mathbf{b})$ , where  $\mathbf{a}$  and  $\mathbf{b}$  are vectors w.r.t.  $t$ . In term of the explicit solution in Theorem 1,  $\|\angle(\beta_1 - \phi_1)\|, \|\angle(\phi_1 - \theta_1)\| \in [0, \frac{\pi}{2}]$  and  $\sin(\beta_1 - \phi_1) \sin(\phi_1 - \theta_1) \geq 0$  such that  $\frac{d}{dt} \cos(\beta_i - \phi_i) \geq 0$ . Since  $A_1$  is in a blocking mode,  $\phi_1 \neq \theta_1$  such that  $\frac{d}{dt} \cos(\beta_i - \phi_i) = 0$  if and only if  $\beta_1 = \phi_1$ . Since  $\|\angle(\beta_1 - \theta_1)\| \in [0, \frac{\pi}{2}]$ ,  $\|\angle(\beta_1 - \phi_1)\|$  will decrease in the blocking mode. Therefore, it is demonstrated  $\phi_i$  converge to  $\beta_i$  when  $A_i \in \mathcal{A}$  is in blocking mode.

Assuming  $A_i \in \mathcal{A}$  is in the blocking mode,  $\theta_i = \beta_i + s\Delta$  for  $s = \{-1, 1\}$ . As demonstrated above,  $\phi_i$  converges to  $\beta_i$ . Once  $\phi_i = \beta_i$ ,  $A_i$  will switch to the opposite correction, i.e.,  $\theta_i = \beta_i - s\Delta$ . However,  $\phi_j \neq \beta_j$  implies that  $A_j$  will keep the previous direction. After this moment,  $w \neq 0$  after  $\phi_i = \beta_i$  such that blocking mode is broken. Thus, Corollary 2 is proved.

#### F. Calculation of Blocking Duration

Fig. 12: Geometric diagram of the blocking duration.  $l_a$ ,  $l_{T1}$  and  $l_{T2}$  are parallel.

Colorary 2 implies that the current blocking mode will be resolved autonomously once the two airplanes become collinear with either target. As the geometric relationship shown in Fig. 12, the blocking duration relies on the earliest collinearity of  $l_a$  with either  $L_{T_1}$  or  $L_{T_2}$ . Therefore,  $T > \frac{\min(L_1, L_2)}{v}$ . As shown in the figure,  $L_i = \|\mathbf{x}_i - \mathbf{T}_i\| \cos(\beta_i - \phi_i)$  for  $i \in \{1, 2\}$ . During the blocking, the distance of airplanes is converging to  $r$ . In terms of the triangle inequality theorem, the actual path is less than  $\min(L_1, L_2) + \|\mathbf{x}_1 - \mathbf{x}_2\| - r$ . Therefore,  $T < \frac{\min(L_1, L_2) + \|\mathbf{x}_1 - \mathbf{x}_2\| - r}{v}$ . To sum up, the lower and upper bound of the blocking duration are calculated to assess the impact of the blocking mode.

### G. Duration Estimation in Adaptive Priority

Furthermore, we evaluate the durations of three options to determine the optimal unblocking priority. Based on the geometric relationship in Fig. 11, the durations for the three decisions can be approximated as follows:

$$T_a \approx \frac{1}{v} [2 \min(\|\mathbf{x}_1 - \mathbf{T}_1\| \cos(\beta_1 - \phi_1), \|\mathbf{x}_2 - \mathbf{T}_2\| \cos(\beta_2 - \phi_2)) + \sqrt{\|\mathbf{T}_1 - \mathbf{x}_c\| - r^2} + \sqrt{\|\mathbf{T}_2 - \mathbf{x}_c\| - r^2} + \pi r],$$

$$T_b \approx \frac{1}{v} [\|\mathbf{T}_1 - \mathbf{x}_1\| + \|\mathbf{T}_2 - \mathbf{x}_1\| + \pi r],$$

$$T_c \approx \frac{1}{v} [\|\mathbf{T}_1 - \mathbf{x}_2\| + \|\mathbf{T}_2 - \mathbf{x}_2\| + \pi r],$$

where  $\mathbf{x}_c = \frac{\mathbf{x}_1 + \mathbf{x}_2}{2}$ . The adaptive priority scheme compares the approximate durations of three decisions and selects the optimal one for the blocking resolution strategy. Although the duration estimations are approximate and the final decision may not be optimal, the adaptive priority based on this duration estimation can statistically improve the utility.